

**Liu J, Ren W, Tian GY, Gao B, Wang YZ, Zhang J, Shaw B, Yin A, King-Alale NO.**

**[Non-destructive Evaluation of Early Contact Fatigue Using Eddy Current Pulsed Thermography.](#)**

***IEEE Sensors Journal* 2015, 15(8), 4409-4419.**

**Copyright:**

© 2015 IEEE. Personal use of this material is permitted. Permission from IEEE must be obtained for all other uses, in any current or future media, including reprinting/republishing this material for advertising or promotional purposes, creating new collective works, for resale or redistribution to servers or lists, or reuse of any copyrighted component of this work in other works.

**DOI link to article:**

<http://dx.doi.org/10.1109/JSEN.2015.2416394>

**Date deposited:**

06/05/2015

# Nondestructive Evaluation of Early Contact Fatigue Using Eddy Current Pulsed Thermography

Jia Liu, Wenwei Ren, Gui Yun Tian, *Senior Member, IEEE*, Bin Gao, *Senior Member, IEEE*, Yizhe Wang, Jishan Zhang, Brian Shaw, Aijun Yin, *Member, IEEE*, and Naomi Omoyeni King-Alale

**Abstract**—Cyclic loading can lead to fatigue damage on the surface or subsurface of a gear tooth. In order to evaluate the contact fatigue damage, this paper applies eddy current pulsed thermography (ECPT) for fatigue damage characterization at different intervals of the loading cycle. The challenging task of fatigue evaluation is one of solving the qualitative microstructure state characterization before microcrack initiation. This paper proposes the thermooptical flow entropy tracking method to trace the heat flow and characterize the degree of fatigue damage while in this status no macrodefects appears using ECPT. In addition, the thermooptical flow is mathematically modeled to yield several desirable unique properties to evaluate minor variations in the microstructure of the material during the fatigue process. The nondestructive evaluation of fatigue damage with ECPT thermooptical flow is derived. The relationship between the entropy of thermooptical flow and the degree of contact fatigue at an early stage is established. The experimental study validates that the proposed method can detect and characterize the implicit damage and that the entropy of thermooptical flow is highly correlated with fatigue cycles which has the potential to evaluate the degree of fatigue damage.

**Index Terms**—D. Non-destructive testing, C. eddy current pulsed thermography, B. fatigue damage, A. gear failure.

## I. INTRODUCTION

**D**UE to high transmission efficiency, accurate transmission ratio, and high power ranges, the gear mechanism is widely used in industrial products. One of the most common

modes of gear failure is contact fatigue damage which is commonly manifested as the initiation and progression of micro-pitting on the flanks of gear teeth [1]. Progressive micro-pitting is the main mode of contact fatigue damage in gears [2]–[7]. This form of fatigue can introduce non-uniform high stress at the contact points and can make gear rotation more noisy, less efficient and prone to gross fatigue failure. Contact fatigue failure normally end with sudden breakage of the gear teeth by crack propagation initiated from the gear flank [1]. Hence, contact fatigue evaluation becomes a major consideration in gear design, state measurement and life prediction.

A wide range of Non-Destructive Testing and Evaluation (NDT&E) methods have been employed for fatigue measurement. For example, the magnetic Barkhausen noise technique has been applied for evaluation of contact fatigue damage and bending fatigue on gears [8]. Another study has shown that substantial acoustic harmonic generation can be obtained from dislocation dipoles generated during plastic deformation and fatigue [9]. Fatigue damage in thick composites can also be detected by pulse-echo ultrasonics [10]. The remnant magnetisation method and eddy current sensors array can also be used for fatigue evaluation in austenitic steel [11], [12]. Since different NDT&E techniques have different characteristics, the integration of different NDT&E techniques to achieve high performance of fatigue defect detection is required [13], [14]. The use of thermography based fatigue detection has the potential for accurate non-contact inspection of a large area within a short time, as well as large standoff distances for a wide range of materials, including: glass fiber, carbon fiber composites, and metallic materials [15]–[19]. In addition, current techniques including lock-in, pulsed optical excitation thermographic techniques which cause heating uneven, cannot tackle the issue of early fatigue damage detection. Furthermore, only the heat deposited the thermal effusively, the defect depth, the thermal diffusivity of the sample is considered by using pulsed thermography and lock-in thermography. Eddy current methods are sensitive to surface and sub-surface defects, but the detection range is restricted by penetration depth. Combining both eddy current and thermography techniques enables fatigue damage to be evaluated with its unique advantages. The technique is known as eddy current pulsed thermography (ECPT) or pulsed eddy current (PEC) stimulated thermography [20]. This technique applies a high current electromagnetic pulse to the conductive material

Manuscript received February 3, 2015; accepted March 12, 2015. This work was supported in part by the National Natural Science Foundation of China under Grant 51377015 and Grant 61401071, in part by the National Scholastic Athletics Foundation under Grant U1430115, in part by the Sichuan Science and Technology Department under Grant 2013HH0059, in part by the China Post Doctoral Program under Grant 136413, and in part by the Seventh Framework Program through the Health Monitoring of Offshore Wind Farms Project. The associate editor coordinating the review of this paper and approving it for publication was Dr. Stefan J. Rupitsch. (*Corresponding authors: Wenwei Ren and Gui Yun Tian.*)

J. Liu, W. Ren, B. Gao, Y. Wang, and N. O. King-Alale are with the School of Automation Engineering, University of Electronic Science and Technology of China, Chengdu 611731, China (e-mail: liujia617200@163.com; kgwrrww@uestc.edu.cn).

G. Y. Tian is with the School of Automation Engineering, University of Electronic Science and Technology of China, Chengdu 611731, China, and also with the School of Electrical and Electronic Engineering, Newcastle University, Newcastle upon Tyne NE1 7RU, U.K. (e-mail: g.y.tian@ncl.ac.uk).

J. Zhang and B. Shaw are with the School of Mechanical Engineering and System, Newcastle University, Newcastle upon Tyne NE1 7RU, U.K.

A. Yin is with the State Key Laboratory of Mechanical Transmission, College of Mechanical Engineering, Chongqing University, Chongqing 400020, China.

Color versions of one or more of the figures in this paper are available online at <http://ieeexplore.ieee.org>.

Digital Object Identifier 10.1109/JSEN.2015.2416394

under inspection. The heat is not limited to the sample surface; rather it can reach a certain depth, which is governed by the skin depth of eddy current. ECPT focus the heat on the defect due to friction or eddy current distortion, which increases the temperature contrast between the defective region and defect-free areas [21]. Therefore, electrical conductivities and the permeability are other two parameters which need to be considered by using Eddy Current Pulsed Thermograph. ECPT can enhance a specific excitation direction to optimise the directional evaluation along the defect orientation which is more effective for geometrically complex components providing a greater indication of surface cracks [22]–[24]. In addition, ECPT allows area imaging of defects without scanning and enables detection of not only magnetic and non-magnetic metals, but also reinforced composites with weak conductivity [25], [26] by using a higher operating frequency.

In our previous work, ECPT has been applied to detect and evaluate defects for gear fatigue measurement and monitoring [27]. For example, the Principle Component Analysis (PCA) is used for fatigue defect pattern extraction, which emphasis uncorrelation of each extracted basis patterns and it is sensitive to detect the macro defects as been proved effectively to separate singular patterns between non-defect and defect region [21]. However, techniques for pixel selection for characterisation around a fatigue damage are difficult to obtain a reliable solution [28]. In addition, current methods of ECPT cannot tackle the issue of early fatigue damage detection during the fatigue process, especially before initiation of micro-cracks.

To overcome these issues, this study proposes the thermo-optical flow entropy method for transient thermal images of ECPT for contact fatigue evaluation [29]–[33]. The optical flow (OF) involves tracking the heat flow across a thermal image sequence [29]–[31], which are modelled as thermo-optical flow (TOF) that can be further extended to quantify heating propagation in gear samples. TOF has been proved quite sensitivity to the property variation of material due to the vary of both heating propagation and volume of heat [26]. In order to quantitatively analyse these heat flows, the entropy of thermo-optical flow is calculated to quantify the differences of heat propagation caused by material changes (fatigue process) for the assessment of fatigue failure [32]–[36]. Therefore, this method is very sensitive for the minor fatigue damage at the early age of contact fatigue process. The relationships between thermo-optical flow entropy and the degree of fatigue are established.

The rest of this paper has been organised as follows. Firstly, specimens, and the method of thermo-optical flow entropy are introduced in Section II. The experimental study and numerical analysis of material features at different fatigue times are provided in Section III. Finally, conclusions and further work are outlined in Section IV.

## II. METHODOLOGY

### A. Systematic Diagram of the Approach

The method for quantitative feature extraction of fatigue characterisation is outlined in Figure 1. It involves several

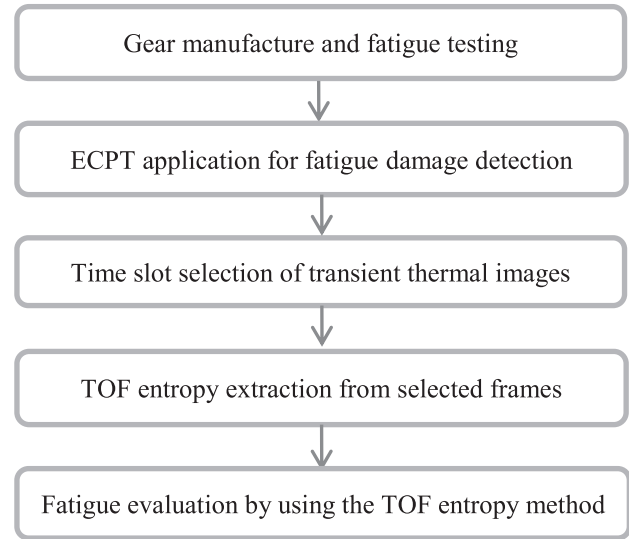


Fig. 1. Systematic diagram of the approach.

stages that include thermal image sequence capture, image pre-processing and selection of an optimal time frame to be used, thermo-optical flow computation, thermo-optical flow (TOF) entropy computation and fatigue evaluation.

### B. Thermal Transient Pattern

The concept of optical flow was first studied in the 1940s and is widely used for estimating velocity fields and object tracking [34]. In this paper, optical flow is applied and used to characterise heating flow between adjacent thermography frames. The thermal transient pattern from ECPT for gear health states during the fatigue process is of primary importance to the structural integrity of gears [27].

Firstly, optical flow is calculated to trace motion between two thermal images captured at times  $t$  and  $t + \Delta t$ . It is based on local Taylor series approximations of the image signal; that is, they use partial derivatives with respect to the spatial and temporal coordinates. For this case, a thermal image sequence is seen as a three dimensional matrix with respect to location  $x$  and  $y$ , and time  $t$ . A vector at location  $(x, y, t)$  with intensity (temperature in this paper)  $I(x, y, t)$  will have moved by  $\Delta x, \Delta y$  after  $\Delta t$  between the two transient images, which can be given [31]:

$$I(x, y, t) = I(x + \Delta x, y + \Delta y, t + \Delta t) \quad (1)$$

In this paper, the displacement between two images represents the temperature variation, which reflects heat propagation. Assuming the displacement is small, the image constraint at  $I(x, y, t)$  with the Taylor series can be developed to:

$$\begin{aligned} & I(x + \Delta x, y + \Delta y, t + \Delta t) \\ &= I(x, y, t) + \frac{\partial I}{\partial x} \Delta x + \frac{\partial I}{\partial y} \Delta y + \frac{\partial I}{\partial t} \Delta t + o(\Delta x^2, \Delta y^2, \Delta t^2) \end{aligned} \quad (2)$$

From these equations, it follows that:

$$\frac{\partial I}{\partial x} \Delta x + \frac{\partial I}{\partial y} \Delta y + \frac{\partial I}{\partial t} \Delta t = 0 \quad (3)$$

Or

$$\frac{\partial I}{\partial x} \frac{\Delta x}{\Delta t} + \frac{\partial I}{\partial y} \frac{\Delta y}{\Delta t} + \frac{\partial I}{\partial t} \frac{\Delta t}{\Delta t} = 0 \quad (4)$$

results in:

$$\frac{\partial I}{\partial x} v_x + \frac{\partial I}{\partial y} v_y + \frac{\partial I}{\partial t} v_t = 0 \quad (5)$$

Where  $v_x$  and  $v_y$  are the  $x$  and  $y$  components of the velocity or optical flow of  $I(x, y, t)$  and  $\partial I/\partial x$ ,  $\partial I/\partial y$  and  $\partial I/\partial t$  are the derivatives of the image at  $(x, y, t)$  in the corresponding directions.  $I_x$ ,  $I_y$  and  $I_t$  can be written for the derivatives in the following equation (6).

$$I_x v_x + I_y v_y = -I_t \quad (6)$$

As the fatigue damage occurs at the area that suffers contact fatigue, the thermal and electrical conductivities of samples are varied [37]–[39]. Thus, both the spatial and transient of heat distribution is non-uniform at these areas. In order to identify these regions, the optical flow is used to track the heat flow for fatigue damage characterization. The heat conduction equation of a specimen caused by a Joule heating source is governed by:

$$\rho C_P \frac{\partial T}{\partial t} = Q + \nabla(k \nabla T) \quad (7)$$

Where  $\rho$ ,  $C_P$ , and  $k$  are density, heat capacity, and thermal conductivity respectively. Furthermore,  $T$  denotes the temperature of the sample,  $Q$  denotes the generated resistive heat and  $t$  means time.

During the heating period, the electrical conductivity and thermal conductivity affect the temperature of the surface such that the Joule heating dominates in the heating period. This phenomenon shows that the bigger the eddy current density is, the higher the obtained temperature will be. The largest value is located in the place which has the largest current density at the end of the Joule heating. At the cooling period, the heat diffusion is varied at the areas that have suffered contact fatigue and this is mainly lead by thermal conductivity. Therefore, the cooling period is a better choice to analyse the process of heat diffusion. Furthermore, the faster temperature (or TOF) changes appear at the cooling period and more explanation can be found in [26].

During the cooling period, where  $Q$  is zero, then, formula (6) leads to:

$$\rho C_P \frac{\partial T}{\partial t} = \nabla(k \nabla T) \quad (8)$$

The intensity  $I(x, y, t)$  is captured by the IR camera which can be used to characterize the thermal spatial and transient behaviour of the sample [26]. IR camera is sensitive to surface and sub-surface defects. The relationship between the intensity  $I$  and the temperature  $T$  can be given as  $I \propto T$  and the first derivative with respect to time,  $t$ , can be given as  $\frac{\partial I}{\partial t} \propto \frac{\partial T}{\partial t}$ . Therefore, the formula (9) can be derived from the equation (6):

$$-\frac{\partial T}{\partial t} \propto (I_x v_x + I_y v_y) \quad (9)$$

Where  $\varepsilon$  is a constant to show the proportional relationship between both sides of the equation.

Then, the following formula (10) can be derived from the formula (8) and formula (9):

$$(I_x v_x + I_y v_y) \propto \frac{-\nabla(k \nabla T)}{\rho C_P} \quad (10)$$

From formula (6) and (10), the relationship between intensity  $I(x, y, t)$ , the temperature of the sample, optical flow is established. Thus, the thermo-optical flow (TOF) is modelled to track the heat flow to characterize the fatigue damage.

The formula (10) in which there are two unknowns, cannot be solved as such thermo-optical flow. The Horn–Schunck method is used for the implementation, where the flow is formulated as a global energy functional which is solved through minimisation.  $\vec{F} = [V_x, V_y]^T$  is the thermo-optical flow (TOF) vector:

$$E = \iint [(I_x V_x + I_y V_y + I_t)^2 + \alpha^2 (|\nabla V_x|^2 + |\nabla V_y|^2)] dx dy \quad (11)$$

Where the smoothness weight  $\alpha > 0$  serves as a regularisation parameter: larger values for  $\alpha$  result in a stronger penalisation of large flow gradients and lead to smoother flow fields.

Due to the Horn–Schunck algorithm being an ill-posed problem, the value of  $V_x$  and  $V_y$  is estimated through to the  $n + 1$  iteration. The TOF vector can be estimated as  $[U, V]^T$  with  $n + 1$  iterations [30], [31].

### C. The Feature of Thermo-Optical Flow Entropy Extraction

In order to visually analyse heat flows, the entropy is calculated from the thermo-optical flow field to quantify the differences of heat propagation caused by material structure change (fatigue process). Entropy has been widely used in quantum mechanics to characterize the degree of uncertainty in the system. Traditionally, the uncertainty in a collection of possible states  $a_i$  with corresponding probability distribution  $p(a_i)$  is given by its entropy  $H(a)$  [35]:

$$H(a) = -\sum p(a_i) \log_2(p(a_i)) \quad (12)$$

called the Shannon entropy [40], where  $a$  means the collection of states  $a_i$ .

This paper proposes a thermo-optical flow entropy driven method to track the heat flow and quantify the degree of fatigue across a thermal image sequence. As the fatigue damage appears at the area that suffers contact fatigue, the property and micro-structure of the material is changed during the fatigue process. Electrical conductivity, thermal conductivity and magnetic permeability become non-uniform at the area that suffers contact fatigue. Thus, the heat distribution is non-uniform at these areas. The thermo-optical flow entropy method is used to trace the disorder of the heat distribution which is directly associated with fatigue.

Thermo-optical flow image sequences are seen as a three dimensional matrix with respect to location  $x$  and  $y$ , and time  $t$  and the extracted thermo-optical flow field between

$t$  and  $t + \Delta t$  times is seen as a two dimension matrix with respect to location  $x$  and  $y$ . Thus, thermo-optical flow of a pixel can be expressed as  $u(i, j)$  and  $v(i, j)$ , where  $i$  and  $j$  is the value of location  $x$  and  $y$ .

Generally, the formula of thermo-optical flow entropy can be defined as:

$$H(u) = - \sum p(u(i, j)) \log_2(p(u(i, j))) \quad (13)$$

$$H(v) = - \sum p(v(i, j)) \log_2(p(v(i, j))) \quad (14)$$

where  $p$  is the probability of thermo-optical flow.

Due to only certain regions of the thermo-optical flow being considered, a specific range of the formula for thermo-optical flow containing contact information of the gear teeth can be set up. This range can be defined as  $\sum_{i=m1}^{m2} \sum_{j=n1}^{n2} u(i, j)$  and  $\sum_{i=m1}^{m2} \sum_{j=n1}^{n2} v(i, j)$  where  $m1 < m2$ ,  $n1 < n2$  and  $m2$ ,  $n2$  is less than the size of thermo-optical flow of the thermal image. So the formula (14) and (15) can be defined as:

$$H(u) = - \sum_{i=m1}^{m2} \sum_{j=n1}^{n2} p(u(i, j)) \log_2(p(u(i, j))) \quad (15)$$

$$H(v) = - \sum_{i=m1}^{m2} \sum_{j=n1}^{n2} p(v(i, j)) \log_2(p(v(i, j))) \quad (16)$$

and  $p$  can be defined as:

$$p(u(i, j)) = \frac{u(i, j)}{\sum_{i=m1}^{m2} \sum_{j=n1}^{n2} u(i, j)} \quad (17)$$

$$p(v(i, j)) = \frac{v(i, j)}{\sum_{i=m1}^{m2} \sum_{j=n1}^{n2} v(i, j)} \quad (18)$$

So the formula (16) and (17) can be defined as:

$$H(u) = - \sum_{i=m1}^{m2} \sum_{j=n1}^{n2} \frac{u(i, j)}{\sum_{i=m1}^{m2} \sum_{j=n1}^{n2} u(i, j)} \times \log_2\left(\frac{u(i, j)}{\sum_{i=m1}^{m2} \sum_{j=n1}^{n2} u(i, j)}\right) \quad (19)$$

$$H(v) = - \sum_{i=m1}^{m2} \sum_{j=n1}^{n2} \frac{v(i, j)}{\sum_{i=m1}^{m2} \sum_{j=n1}^{n2} v(i, j)} \times \log_2\left(\frac{v(i, j)}{\sum_{i=m1}^{m2} \sum_{j=n1}^{n2} v(i, j)}\right) \quad (20)$$

Therefore, the entropy of the thermo-optical flow, which is defined as equations (19) and (20), measures the disorder of the heat flow to quantify the fatigue damage.

### III. RESULTS AND DISCUSSION

#### A. Sample Preparation and Experiments Setup

Gear manufacture and fatigue testing were carried out at the Design Unit – Gear Technology Centre, Newcastle University. The 6 mm module helical test gears had a 44 mm facewidth. The gears were manufactured from an 18CrNiMo7 steel bar, as shown in Figure 2. The gears were tested on a 160 mm centre distance back-to-back contact fatigue test rig at 3000 rpm (pinion) with a BGA test oil at 90 °C [1]. A stepwise micro-pitting test was employed which involves running gears at incrementally increasing contact stress levels with each stage running for up to 8 million cycles, as illustrated in Figure 3.

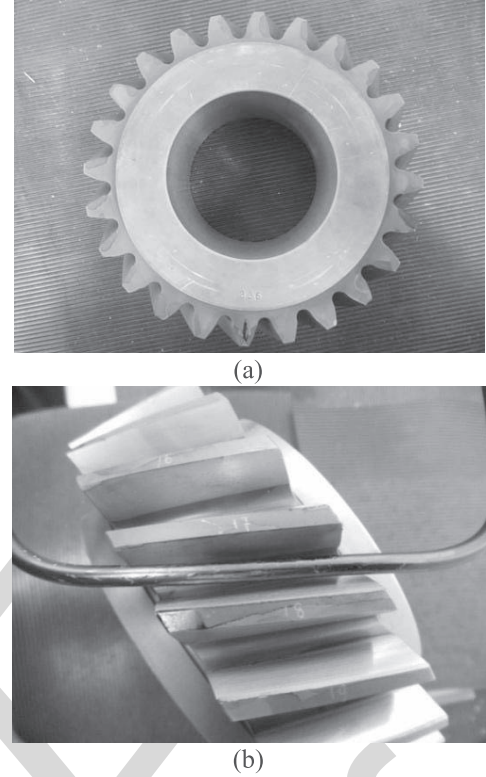


Fig. 2. (a) The Gear sample. (b) Fatigue test gear with inductor coil.

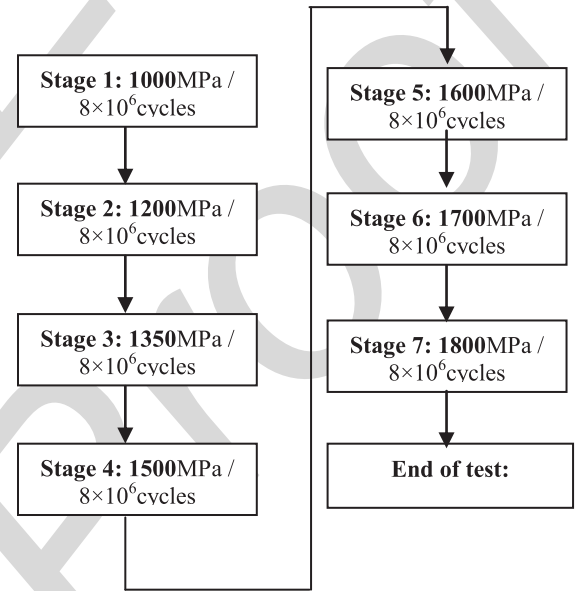


Fig. 3. Procedure of the stepwise micro-pitting test.

ECPT deviation was measured after each stage of running. Comparing with the service life of the gear, in this accelerated life experiment, the fatigue testing time is short before initial micro-crack initiation when microstructure of the tooth flank is modified and low levels of fatigue damage is created. During the fatigue process, the microstructure of the gear is changed. These changes lead to a considerable decrease in thermal conductivity, electrical conductivity and magnetic permeability [37]–[39]. The relationship between the heat



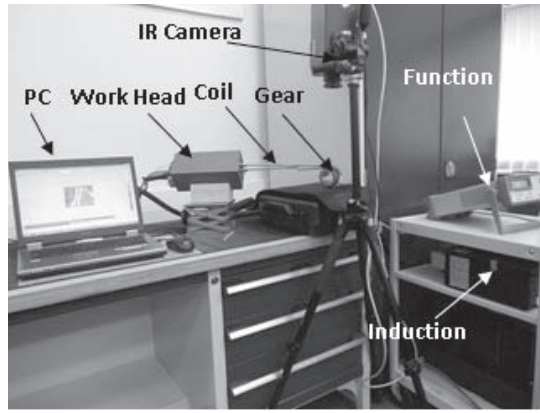


Fig. 4. ECPT experimental system.

distribution and these parameters can be established by using the pulsed eddy current thermography method. This paper proposes a thermo-optical flow entropy method to trace the change of heat flow to characterize the degree of fatigue damage before micro-crack initiation.

The eddy current pulsed thermography (ECPT) is shown in Figure 4. An Easy heat 224 instrument from Cheltenham Induction Heating is used for coil excitation. The Easy heat has a maximum excitation power of 2.4 kW, a maximum current of 400 Arms and an excitation frequency range of 150-400 kHz (200 Arms and 256 kHz were used during this study). This measurement system has a quoted rise time (the heating period to full power) of 5ms, which was verified experimentally. Water cooling of the coil is implemented to counteract direct heating of the coil [22]–[24].

An SC7500 IR camera is a Stirling cooled camera with a  $320 \times 256$  array of  $1.5\text{-}5\mu\text{m}$  InSb detectors. This camera has a sensitivity of  $<20$  mK and a maximum full frame rate of 383 Hz, with the option to increase the frame rate with windowing of the image. A rectangular coil is constructed to apply directional excitation. This coil is made of 6.35 mm high conductivity hollow copper tubing. During the experiment, only one edge of the rectangular coil is used to stimulate eddy currents to the sample below. In this study, the frame rate was 383 Hz with a  $320 \times 256$  array and 2s videos were recorded in the experiments.

When the gear teeth are tested to analyse the level of contact fatigue, the thermal image sequences contain the information of two gear teeth, captured by the SC7500 IR camera. The two gear flanks are defined as fatigue contact tooth flank and fatigue non-contact tooth flank. The fatigue contact tooth flank suffers contact fatigue, whereas the fatigue non-contact tooth flank does not suffer any contact fatigue and is a direct comparison with the fatigue contact tooth flank. As shown in Figure 5, when the SC7500 IR camera is used to capture the thermal image sequences, irradiation angles are taken for analysis. These two tooth flanks are taken to evaluate the fatigue damage.

#### B. Time Slot Selection of Transient Thermal Images

As shown in Figure 6 (a), the gradation changes (as marked by the rectangular region) across time. The information of the

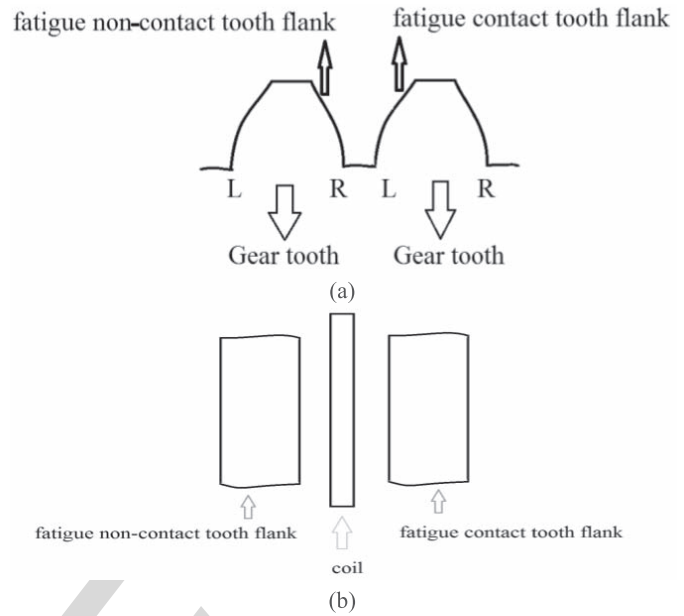


Fig. 5. (a) Two gear teeth. (b) A capturing angle of the infrared camera on gear teeth.

marked areas is displayed to explore how to properly select the specific transient time period for the optimal comparison between fatigue failures with high sensitivity. As shown in Figure 6, the slope of the falling edge is larger and the first derivative of transient pattern varies sharply [23]. This characteristic can be exploited for further NDE. In this paper, TOF is extracted from two images of the transient thermal images. Based on faster temperature (or TOF) changes at the falling edge, the beginning of the cooling stage is a viable region for selection to allow further analysis and more specific explanation on how to choose the proper frames can be found in [26]. In this study, 200–250 thermal frames (523–720 ms) are selected for analysis with these frames marked by the rectangular box shown in Figure 6 (a).

#### C. Deriving Thermo-Optical Flow From Transient Thermal Image Sequences

By deriving the thermo-optical flow from the thermal image, it is clear to see the process of heat diffusion across the gear surface. Thermo-optical flow is calculated to trace the heat motion between two thermal images. In order to demonstrate the process of the heat flow from another angle, thermo-optical flow is illustrated using the vector as shown in Figure 7 (a) and (b), the pseudo colour images as shown in Figure 7 (d) and (e). In order to avoid the background image for fatigue damage detection, only the measured gear is considered and the thermo-optical flow value on the surrounding background is set to zero.

In Figure 7, the distribution of thermo-optical flow on the gear surface during the cooling period is analysed. As shown in Figure 7 (c), a TOF vector can be decomposed into two directions. From Figure 7 (a) and (b), it is shown that the TOF have the uniform distribution and non-disorder direction at the non-contact tooth flank. Because of the microstructure

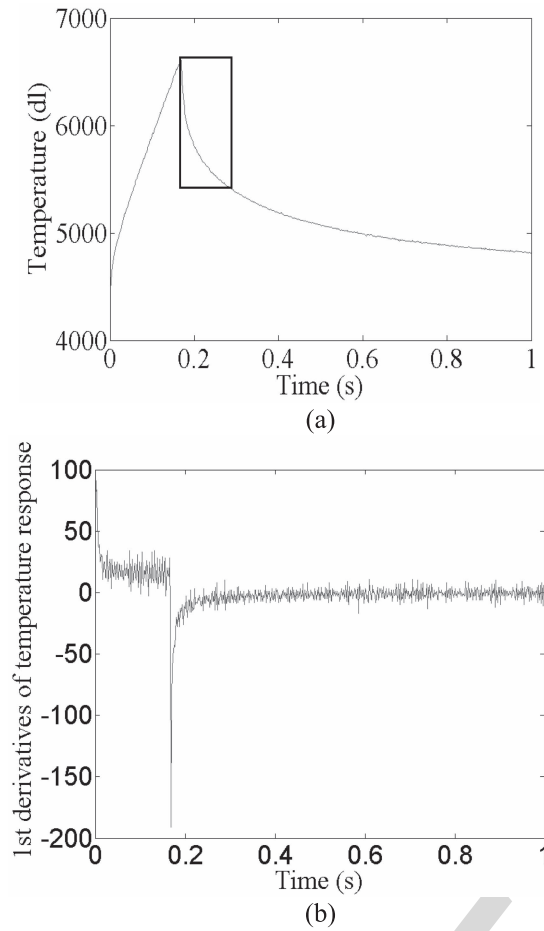


Fig. 6. Transient thermal behaviour for time slot selection. (a) The transit response using the images at Stage 7, where the horizontal axis represents time and the vertical axis represents temperature greyscale. (b) The first derivative of the transit response using the images at Stage 7, where the horizontal axis represents time and the vertical axis represents the first derivative of the temperature curve.

of the non-contact tooth flank does not vary, the properties of electrical conductivity, thermal conductivity and magnetic permeability of the non-contact tooth flank remain in the originated state. Thus, the heat distribution is reflected as approximately uniform at the cooling stage of transient thermal behaviour. However, comparing with the TOF of the fatigue non-contact tooth flank, the singular values of TOF appear on the fatigue contact tooth flank. These mean that the conductive properties of the material and the thermal conductivity of the permeability become different and contact fatigue appears at certain areas of the fatigue contact tooth flank. The heat therefore converges on these places where the contact fatigue initiated and the singular values of TOF are seen at these locations. Especially, these phenomenon become obvious in the  $v$  direction.

Thermo-optical flow is calculated to trace motion of heat flow between two thermal images captured at times  $t$  and  $t + \Delta t$ . As the fatigue damage is slight, mirror reflection would influence the defect detection by using the ECPT method. In this paper, the differentiation method is used to eliminate the influence of surface curvature and thermal emissivity. Furthermore, as mirror reflection of a Gear does

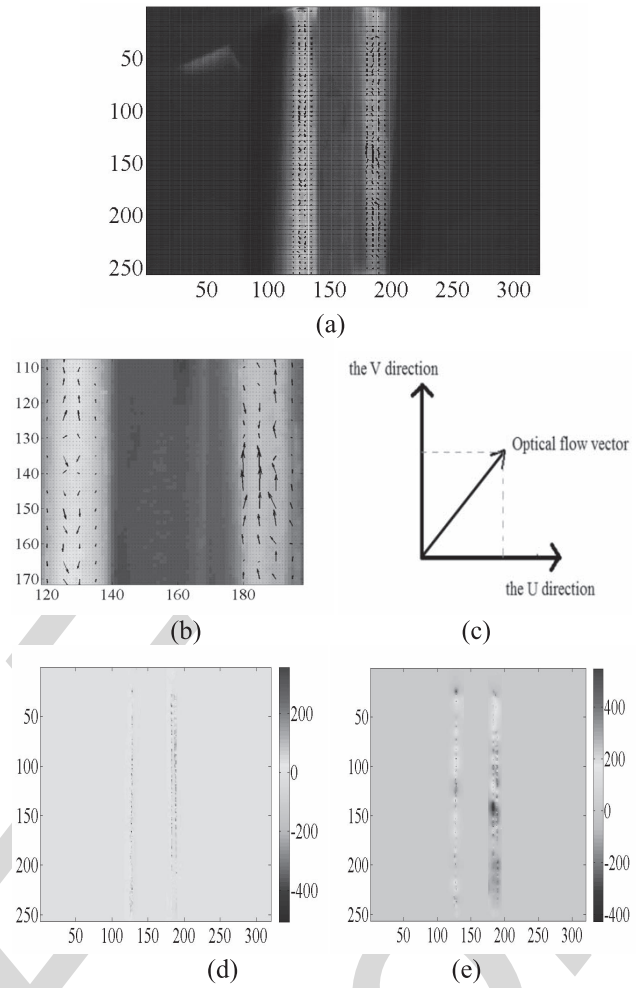


Fig. 7. (a) Thermo-optical flow distribution at Stage 7 (the size of arrows indicate the thermo-optical flow values and the direction of arrow indicates the thermo-optical flow direction). (b) Thermo-optical flow which is amplified from Fig.7 (a). (c) The direction of a OF vector. (d) The pseudo colo images of TOF value in the  $u$  direction at stage 7. (e) The pseudo colo images of TOF value in the  $v$  direction at Stage 7/(Note: the fatigue non-contact tooth flank is on the left, and fatigue contact tooth flank is on the right.)

not change the heat flow, the method of thermo-optical flow can approximately eliminate the effect of mirror reflection. Fatigue behaviour is the cyclic deformation behaviour of metallic materials which always suffer mechanical (electrical) stress or strain effects. In cyclic deformation, as the material structure is damaged, the conductive properties of the material and the thermal conductivity of the permeability are modified. As the fatigue damage can change the velocity and direction of the heat at different areas of the fatigue contact tooth flank as such, the TOF can be used to track the heat flow for fatigue damage detection. From figure 7 (d) and (e), the thermo-optical flow value in the  $u$  direction is always less than the thermo-optical flow value in the  $v$  direction. These mean that the heat always spreads along the gear teeth axis and there is little heat transmission to the air between the teeth. For the adjacent gear teeth, the medium of the heat transmission between the tooth and the adjacent tooth is air. Thus, the speed of heat propagation is slower among the teeth than the heat transmission along the gear tooth. The value of thermo-optical

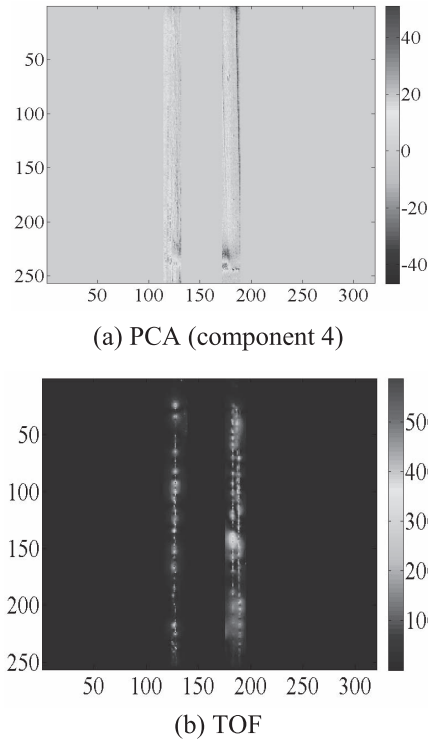


Fig. 8. Two-dimensional pseudo colour images at stage 5: (a) using PCA method and (b) using TOF method. (Note: the fatigue non-contact tooth flank is on the left, and fatigue contact tooth flank is on the right).

flow on the gear teeth is much greater than the value on the surrounding background. Furthermore, the value of thermo-optical flow on the fatigue contact tooth flank using the images at Stage 7 is much greater than the value on the fatigue non-contact tooth flank which does not suffer contact fatigue.

#### D. The Difference Results by Using PCA Method From the Previously Published Work

This paper mainly focus on an extremely challenge task for ECPT to detect and evaluate the micro structure variation of material while in this status no macro defects appears and these property variation region can be considered as the hidden defects. In our previous study, several algorithms is developed to handle the macro defects such as cracks, impact damage, delamination and so on. To emphasis the contribution of this work, the proposed method with our latest previous study is compared [21] which uses pattern separation method for crack detection. Specifically, the Principle Component Analysis (PCA) is used for defect pattern extraction. The Figure 8 show the comparison results.

Figure 8 displays the comparison results of detecting hidden defects (property variation of material), it can be clearly seen that it is difficult to find obviously singular region between the fatigue non-contact tooth flank and the fatigue contact tooth flank on component 4 by using PCA. Using PCA method, in order to choose the appropriate component which can characterise defect, every component needs to be analyzed. The PCA emphasis uncorrelation of each extracted basis patterns and it is sensitive to detect the macro defects as

been proved effectively to separate singular patterns between non-defect and defect region [21]. This is because when macro defects exist, the path of eddy current is distorted apparently and the resistive heat between defect and nondefect region are different and uncorrelated while this characteristic makes PCA easily extract singular patterns to detect the defects. The Thermo-optical flow is more focus on characterizing the changes of heat flow, and these changes directly link the features with the physical and material properties at the early age of fatigue process. The entropy is calculated from the thermo-optical flow field to quantify the differences of heat propagation caused by material structure change (fatigue process). The thermo-optical flow entropy is very sensitive to characterize the minor gear feature changes at the early age of fatigue process. Specifically, because of the micro-structure of the non-contact tooth flank is not vary, the properties electrical conductivity, thermal conductivity and magnetic permeability of the non-contact tooth flank is retain originated state. Thus, the heat distribution is reflected as approximately uniform at the cooling stage of transient thermal behaviour. However, comparing the TOF of fatigue non-contact tooth flank, the singular values of TOF are appeared at fatigue contact tooth flank. These means the conductive properties of the material and the thermal conductivity of the permeability become different and contact fatigue appear at certain area of fatigue contact tooth flank. Then the heat is converged on these places where the contact fatigue appeared. And the singular values of TOF are appeared on these places. Especially, these phenomenons become obvious in the  $v$  direction. Then thermo-optical flow entropy is extracted to quantitatively analyse these heat flows.

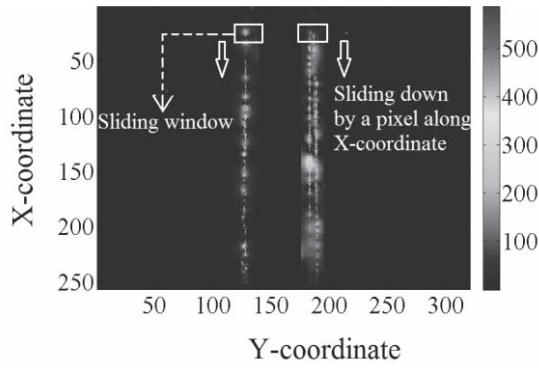
#### E. Extracting TOF Entropy

In order to reflect the changes of thermo-optical flow in another angle, thermo-optical flow entropy is extracted.

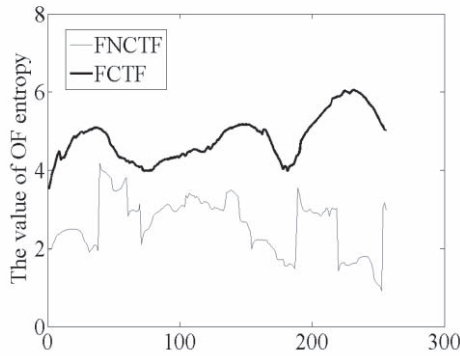
From Figure 9, thermo-optical flow entropy is taken to quantify fatigue damage. In order to capture the specific areas which have been affected by contact fatigue, a sliding window for thermo-optical flow entropy extraction of a small region is taken and analysed as shown in Figure 9 (a). The sliding window is moving by a pixel along the X-coordinate. The size of the sliding window exactly coincides with the size of the measured gear teeth. So with movement of the sliding window, the fatigue damage in some specific areas is detected. When extracting the thermo-optical flow entropy, only the norm of TOF is considered, as shown in Figure 9 (a). As shown in formulas (19) and (20), the location of the sliding window is determined by the value of  $m1$ ,  $m2$ ,  $n1$  and  $n2$ . The entropy of the thermo-optical flow is taken to measure the degree of disorder which directly associates with the level of fatigue.

From Figure 9 (b) and (c), the thermo-optical flow entropy became obviously different of the two gear teeth at stage 5 and stage 7. The value of thermo-optical flow entropy is greater on the fatigue contact tooth flank which suffered contact fatigue. As the heat distribution is uniform at fatigue non-contact tooth flank, the disorder degree of TOF is lower on the fatigue non-contact tooth flank, which characterises



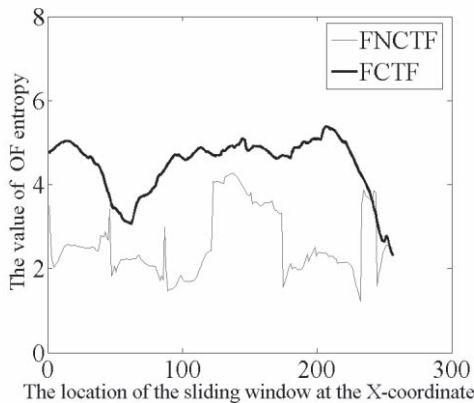


(a)



The location of the sliding window at the X-coordinate

(b) at stage 7



The location of the sliding window at the X-coordinate

(c) at stage 5

Fig. 9. (a) Sliding window for norm of thermo-optical flow at Stage 7. (b) Thermo-optical flow entropy at Stage 7. (c) Thermo-optical flow entropy at stage 5. (Where FNCTF means fatigue non-contact tooth flank, and FCTF means fatigue contact tooth flank.)

can characterise the change of the material microstructure and establish the relationship between thermo-optical flow entropy and the microstructure of gear fatigue at an early stage.

From Figure 9 (b) and (c), the value of thermo-optical flow entropy is higher at stage 7 than at stage 5. This indicates that the degree of fatigue damage increased with the an increase of cyclic loading. From Figure 10, the details of fatigue damage during the fatigue process are analysed.

In order to analyse the variation of fatigue damage as a fatigue test progresses, two-dimensional pseudo colour images of thermo-optical flow in the  $v$  direction and thermo-optical flow entropy at different stages were analysed.

As shown in Figure 10, only the fatigue contact tooth flank is considered. Due to the uncertainty with manually setting of the camera angle, the gear position shows slight variations in the image. At the early stage of the contact fatigue, only the microstructure of the tooth flank is varied and the degree of fatigue damage is small. Especially, the macroscopic crack is not formed during this stage of the fatigue process. Thermo-optical flow is able to track small changes of the microstructure. From Figure 10 (c) to Figure 10 (a), the values of the thermo-optical flow norm become greater on the fatigue contact tooth flank, which corresponds with increasing levels of contact fatigue damage. When the fatigue damage does not appear as on the fatigue non-contact tooth flank, the TOF value is close to zero. On the other hand, the norm of the thermo-optical flow value becomes greater. Positive and negative values of thermo-optical flow represent the heat flow direction along  $v$  direction. The degree of fatigue damage becomes greater and the areas of fatigue damage gradually increase when the fatigue cycles increase. Especially, fatigue damage always appears in the same locations (such as the areas M and N in Figure 10), the degree of fatigue damage to the material structure increases in these locations as the fatigue test progresses. In Figure 10 (d) and (e), thermo-optical flow entropy is extracted at stage 7 and stage 3. The value of thermo-optical flow entropy is higher at stage 7 than the value at stage 3. Slight variations of thermo-optical flow entropy are shown in the Figure 10 (d) and (e). Take area M for example, the highest value of thermo-optical flow entropy is 4.08 at stage 3, where the highest value of thermo-optical flow entropy is 5.08 at stage 7. These results indicate that the degree of the fatigue damage increases at the fatigue contact region as the fatigue test progresses. These results have shown in Figure 10 (d) and (e) are line with that shown in Figure 10 (a), (b) and (c). During the early cyclic deformation, only some of the grains are plastically deformed and the plastic deformation degrees of the grains are different. With increasing fatigue cycles, the extent of plastic deformation of the grains increases and the number of grains which are plastically deformed is also increased. This explains that fatigue damage of the material structure suddenly increases in M and N areas. The areas M and N can be considered as an incubation area of a fatigue crack where physical characteristics are significantly changed in these areas. Furthermore, the fatigue damage is diffused from M and N areas to the surroundings on the gear tooth and fatigue damage thus appears across the whole area of the

the material properties of a gear before fatigue accumulation. At the fatigue contact tooth flank, the heat converges at the places where the singular values of TOF appeared because of the changing microstructure on the fatigue contact tooth flank surface. As the TOF value is quite different between the area where the heat converges and the adjacent area, the degree of disorder is higher. Thermo-optical flow entropy is used to quantify the disorder of the heat flow such that the higher the value of thermo-optical flow entropy, the higher the degree of fatigue damage. Therefore, the thermo-optical flow entropy which traces the motion of heat flow during the fatigue process

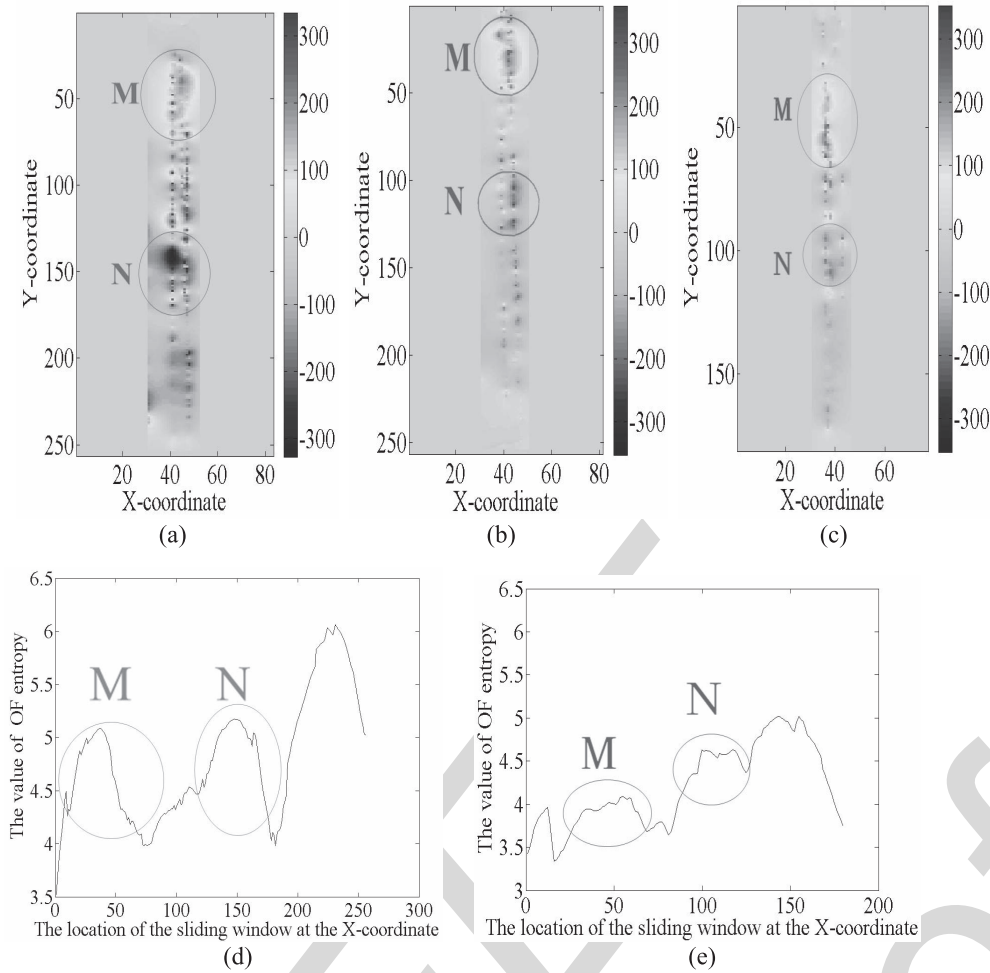


Fig. 10. Two-dimensional pseudo color images of thermo-optical flow in the  $v$  direction at different stages: (a) at Stage 7; (b) at Stage 5; (c) at Stage 3. Thermo-optical flow entropy at different stages: (d) at Stage 7; (e) at Stage 3.

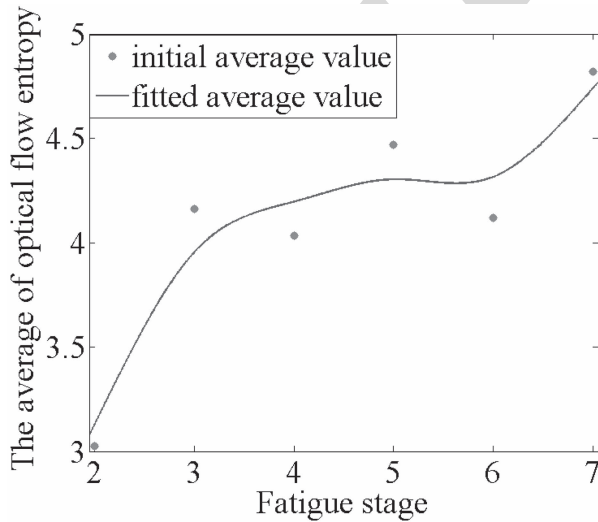


Fig. 11. The curve of average of thermo-optical flow entropy with different fatigue stage where the horizontal axis represents the fatigue stage and the vertical axis represents the average of thermo-optical flow entropy.

structure induces the change of the heat transfer coefficient; 2) the change of the heat transfer coefficient induces the change of the thermo-optical flow velocity; 3) using thermo-optical flow entropy then highlights these changes.

On the basis of the studies above, the degree of fatigue damage can be evaluated. From Figure 9 and Figure 10, the curves of thermo-optical flow entropy have shown the potential to evaluate the degree of fatigue damage. Therefore the average of the thermo-optical flow entropy on gear teeth is focused to derive the conclusion as shown in Figure 11. The fitted average value of thermo-optical flow entropy is used to analyse the change of fatigue damage as the fatigue test progresses. This figure shows the phenomenon of the rise in fatigue damage as the fatigue cycles increase. Thus fatigue damage covered most of the fatigue contact tooth flank.

#### IV. CONCLUSION AND FUTURE WORK

In this paper, the thermo-optical flow entropy has been applied to evaluate the fatigue damage by using ECPT. The relationships between the TOF entropy and the degree of fatigue damage have been analysed. The results show that TOF entropy highly correlated with the level of cyclic fatigue loading. In the future, NDE of a wider array of dedicated samples will be evaluated through multiple parameters such

fatigue contact tooth flank. In this paper, thermo-optical flow entropy is used to underline these changes. This phenomenon can be summarised as: 1) the fatigue damage of the material

as magnetic barkhausen noise etc. Simulations will be carried out to build the relationships between fatigue damage and variation in physical or mechanical properties, mechanical and material states, such as stress/strain and thermal and electrical conductivity.

Furthermore, the spread of fatigue damage and the formation of micro-cracks will be carried out in conjunction with more feature extraction including TOF histogram and pattern, experimental studies for life-cycle assessment and cracking prediction. The demerits/limitations of the present approach over lock-in, pulsed optical excitation thermographic techniques will block some imaging areas due to excitation coils, which will be addressed in future papers.

## REFERENCES

- [1] M. Vaidhianathasamy, B. A. Shaw, W. Bennett, and P. Hopkins, "Evaluation of contact fatigue damage on gears using the magnetic Barkhausen noise technique," in *Electromagnetic Nondestructive Evaluation (XI)*, vol. 38. Amsterdam, The Netherlands: IOS Press, 2008, pp. 98–106.
- [2] P. J. L. Fernandes and C. McDuling, "Surface contact fatigue failures in gears," *Eng. Failure Anal.*, vol. 4, no. 2, pp. 99–107, 1997.
- [3] V. Moorthy and B. A. Shaw, "An observation on the initiation of micro-pitting damage in as-ground and coated gears during contact fatigue," *Wear*, vol. 297, nos. 1–2, pp. 878–884, 2013.
- [4] A. V. Olver, L. K. Tiew, S. Medina, and J. W. Choo, "Direct observations of a micropit in an elastohydrodynamic contact," *Wear*, vol. 256, nos. 1–2, pp. 168–175, 2004.
- [5] W. Dong, Y. Xing, T. Moan, and Z. Gao, "Time domain-based gear contact fatigue analysis of a wind turbine drivetrain under dynamic conditions," *Int. J. Fatigue*, vol. 48, pp. 133–146, Mar. 2013.
- [6] J. Schijve, "The significance of fatigue crack initiation for predictions of the fatigue limit of specimens and structures," *Int. J. Fatigue*, vol. 61, pp. 39–45, Apr. 2014.
- [7] N. R. Paulson, J. A. R. Bomidi, F. Sadeghi, and R. D. Evans, "Effects of crystal elasticity on rolling contact fatigue," *Int. J. Fatigue*, vol. 61, pp. 67–75, Apr. 2014.
- [8] V. Moorthy, B. A. Shaw, and P. Hopkins, "Magnetic Barkhausen emission technique for detecting the overstressing during bending fatigue in case-carburised En36 steel," *NDT & E Int.*, vol. 38, no. 2, pp. 159–166, 2005.
- [9] J. H. Cantrell, "Nondestructive evaluation of metal fatigue using nonlinear acoustics," in *Proc. AIP Conf., Rev. Progr. Quant. Nondestruct. Eval.*, vol. 28, 2009, pp. 19–32.
- [10] A. P. Mouritz, C. Townsend, and M. Z. S. Khan, "Non-destructive detection of fatigue damage in thick composites by pulse-echo ultrasonics," *Compos. Sci. Technol.*, vol. 60, no. 1, pp. 23–32, 2000.
- [11] D. Miu, L. Miu, G. Jakob, and H. Adrian, "Relaxation of remnant magnetisation in YBa<sub>2</sub>Cu<sub>3</sub>O<sub>7</sub>-delta films," *Phys. C-Supercond. Appl.*, vol. 460, no. 2, pp. 1243–1244, 2007.
- [12] X. Chen and T. Ding, "Flexible eddy current sensor array for proximity sensing," *Sens. Actuators A, Phys.*, vol. 135, no. 1, pp. 126–130, 2007.
- [13] R. Grimberg, A. Savin, and R. Steigmann, "Detection and measurement of fatigue in ferromagnetic and austenitic steels using eddy current sensors array," in *Proc. AIP Conf.*, vol. 760, 2004, pp. 1400–1407.
- [14] M. Oka, T. Yakushiji, and M. Enokizono, "Fatigue dependence of residual magnetization in austenitic stainless steel plates," *IEEE Trans. Magn.*, vol. 37, no. 4, pp. 2045–2048, Jul. 2001.
- [15] Z.-F. Yan, H.-X. Zhang, W.-X. Wang, K. Wang, and F.-F. Pei, "Temperature evolution and fatigue life evaluation of AZ31B magnesium alloy based on infrared thermography," *Trans. Nonferrous Met. Soc. China*, vol. 23, no. 7, pp. 1942–1948, 2013.
- [16] M. Ishikawa, H. Hattai, Y. Habuka, R. Fukui, and S. Utsunomiya, "Detecting deeper defects using pulse phase thermography," *Infr. Phys. Technol.*, vol. 57, no. 2, pp. 42–49, Mar. 2013.
- [17] D. Peng and R. Jones, "Modelling of the lock-in thermography process through finite element method for estimating the rail squat defects," *Eng. Failure Anal.*, vol. 28, pp. 275–288, Mar. 2013.
- [18] Z. Zeng, N. Tao, L. Feng, and C. Zhang, "Specified value based defect depth prediction using pulsed thermography," *J. Appl. Phys.*, vol. 112, no. 2, pp. 023112-1–023112-7, 2012.
- [19] B. Gao, A. Yin, G. Tian, and W. L. Woo, "Thermography spatial-transient-stage mathematical tensor construction and material property variation track," *Int. J. Thermal Sci.*, vol. 85, pp. 112–122, Nov. 2014.
- [20] J. Wilson, G. Y. Tian, I. Z. Abidin, S. Yang, and D. Almond, "Modelling and evaluation of eddy current stimulated thermography," *Nondestruct. Test. Eval.*, vol. 25, no. 3, pp. 205–218, 2010.
- [21] B. Gao, L. Bai, W. L. Woo, G. Y. Tian, and Y. Cheng, "Automatic defect identification of eddy current pulsed thermography using single channel blind source separation," *IEEE Trans. Instrum. Meas.*, vol. 63, no. 4, pp. 913–922, Apr. 2014.
- [22] B. Gao, L. Bai, W. L. Woo, and G. Tian, "Thermography pattern analysis and separation," *Appl. Phys. Lett.*, vol. 104, no. 25, pp. 251902-1–251902-5, 2014.
- [23] A. Yin, B. Gao, G. Y. Tian, W. L. Woo, and K. Li, "Physical interpretation and separation of eddy current pulsed thermography," *J. Appl. Phys.*, vol. 113, no. 6, p. 064101, 2013.
- [24] N. Biju, N. Ganesan, C. V. Krishnamurthy, and K. Balasubramaniam, "Simultaneous estimation of electrical and thermal properties of isotropic material from the tone-burst eddy current thermography (TBET) time-temperature data," *IEEE Trans. Magn.*, vol. 47, no. 9, pp. 2213–2219, Sep. 2011.
- [25] L. Cheng, B. Gao, G. Y. Tian, W. L. Woo, and G. Berthiau, "Impact damage detection and identification using eddy current pulsed thermography through integration of PCA and ICA," *IEEE Sensors J.*, vol. 14, no. 5, pp. 1655–1663, May 2014.
- [26] W. Ren, J. Liu, G. Y. Tian, B. Gao, L. Cheng, and H. Yang, "Quantitative non-destructive evaluation method for impact damage using eddy current pulsed thermography," *Compos. B, Eng.*, vol. 54, pp. 169–179, Nov. 2013.
- [27] G. Y. Tian, A. Yin, B. Gao, J. Zhang, and B. Shaw, "Eddy current pulsed thermography for fatigue evaluation of gear," in *Proc. QNDE, USA*, 2013.
- [28] J. Liu, G. Y. Tian, B. Gao, W. Ren, and J. S. Meng, "Investigation of thermal imaging sampling frequency for eddy current pulsed thermography," *NDT & E Int.*, vol. 62, pp. 85–92, Mar. 2014.
- [29] H. W. Haussecker, "Simultaneous estimation of optical flow and heat transport in infrared image sequences," in *Proc. IEEE Workshop Comput. Vis. Beyond Visible Spectrum, Methods Appl.*, 2000, pp. 85–93.
- [30] S.-C. Huang and B.-H. Chen, "Automatic moving object extraction through a real-world variable-bandwidth network for traffic monitoring systems," *IEEE Trans. Ind. Electron.*, vol. 61, no. 4, pp. 2099–2112, Apr. 2014.
- [31] W. Yingchun *et al.*, "Velocity measurement of microchannel flow with micro-PIV using optical flow estimation," in *Proc. IEEE Int. Conf. Electr. Inf. Control Eng. (ICEICE)*, Apr. 2011, pp. 2839–2842.
- [32] A. Antoniouk, K. Keller, and S. Maksymenko, "Kolmogorov–Sinai entropy via separation properties of order-generated  $\sigma$ -algebras," *Discrete Continuous Dyn. Syst.*, vol. 34, no. 5, pp. 1793–1809, 2014.
- [33] H. Deng, Y. Wei, and M. Tong, "Background suppression of small target image based on fast local reverse entropy operator," *IET Comput. Vis.*, vol. 7, no. 5, pp. 405–413, Oct. 2013.
- [34] T. Brox, A. Bruhn, N. Papenberg, and J. Weickert, "High accuracy optical flow estimation based on a theory for warping," in *Proc. 8th Eur. Conf. Comput. Vis.*, vol. 4, Prague, Czech Republic, 2004, pp. 25–36.
- [35] V. Vedral, "The role of relative entropy in quantum information theory," *Rev. Modern Phys.*, vol. 74, no. 1, pp. 197–234, 2002.
- [36] L. Paninski, "Estimation of entropy and mutual information," *Neural Comput.*, vol. 15, no. 6, pp. 1191–1253, 2003.
- [37] M. Naderi and M. M. Khonsari, "On the characterization of thermal-conductivity degradation during torsional fatigue," *Int. J. Thermophys.*, vol. 32, no. 3, pp. 693–703, 2011.
- [38] A. Q. Morrison *et al.*, "Elastic modulus, biaxial fracture strength, electrical and thermal transport properties of thermally fatigued hot pressed LAST and LASTT thermoelectric materials," *Mater. Chem. Phys.*, vol. 134, nos. 2–3, pp. 973–987, 2012.
- [39] Y. Melikhov, C. C. H. Lo, O. Perevertov, J. Kadlecová, D. C. Jiles, and I. Tomas, "Magnetic response to cyclic fatigue of low carbon Fe-based samples," *J. Phys. D, Appl. Phys.*, vol. 35, no. 5, pp. 413–422, 2002.
- [40] B. W.-K. Ling, C. Y.-F. Ho, and P. K.-S. Tam, "Detection of chaos in some local regions of phase portraits using Shannon entropies," *Int. J. Bifurcation Chaos*, vol. 14, no. 4, pp. 1493–1499, 2004.
- [41] S. Pickering and D. Almond, "Matched excitation energy comparison of the pulse and lock-in thermography NDE techniques," *NDT & E Int.*, vol. 41, no. 7, pp. 501–509, 2008.

**Jia Liu** received the B.Sc. degree from the School of Computer and Information Science, Southwest University, Chongqing, China, in 2008. She is currently pursuing the M.Sc. degree in fatigue assessment and life cycle assessment using electromagnetic technique at the University of Electronic Science and Technology of China, Chengdu, China. Her research interests include sensor signal processing, fatigue evaluating, structural health monitoring, and network security.

**Wenwei Ren** was born in 1968. She received the Ph.D. degree from the Sichuan University of China, in 2007. She is currently a Teacher with the University of Electronic Science and Technology of China. She was involved in metal material research and metal fatigue fracture 3-D modeling work, and the feature extraction and analysis of dynamic crack propagation process. She was with the Research Center of Nondestructive Testing, in 2012, which was led by Prof. G.-Y. Tian. Her research includes the electromagnetic nondestructive testing, the fatigue life evaluation, and defect recognition research.

**Gui Yun Tian** (M'01–SM'03) received the B.Sc. degree in metrology and instrumentation and the M.Sc. degree in precision engineering from the University of Sichuan, Chengdu, China, in 1985 and 1988, respectively, and the Ph.D. degree from the University of Derby, Derby, U.K., in 1998. From 2000 to 2006, he was a Lecturer, a Senior Lecturer, a Reader, a Professor, and the Head of the Group of Systems Engineering with the University of Huddersfield, U.K. Since 2007, he has been the Chair Professor of Sensor Technologies with Newcastle University, Newcastle upon Tyne, U.K. He has coordinated several research projects from the Engineering and Physical Sciences Research Council, the Royal Academy of Engineering, and FP7, and also has good collaboration with leading industrial companies, such as Airbus, Rolls Royce, BP, nPower, and TWI. He is currently an Adjunct Professor with the School of Automation Engineering, University of Electronic Science and Technology of China.

**Bin Gao** (M'12–SM'14) received the B.S. degree in communications and signal processing from Southwest Jiao Tong University, Chengdu, China, in 2005, the M.Sc. (Hons.) degree in communications and signal processing, and the Ph.D. degree from Newcastle University, Newcastle, U.K., in 2011. He was a Research Associate with Newcastle University from 2011 to 2013, where he was involved in wearable acoustic sensor technology. He is currently an Associate Professor with the School of Automation Engineering, University of Electronic Science and Technology of China, Chengdu. His current research interests include sensor signal processing, machine learning, data mining for nondestructive testing, and evaluation. He is a very active Reviewer for many international journals and long standing conferences.

**Yizhe Wang** received the B.Sc. degree in physics from Shenyang Normal University, Shenyang, China, in 2012, and the M.E. degree in instrument science and technology from the University of Electronic Science and Technology of China, Chengdu, China, in 2014, where he is currently pursuing the Ph.D. degree in quantitative fatigue assessment and health state monitoring using eddy current pulsed thermography. His current research interests include sensor design, fatigue damage, quantitative nondestructive testing, and evaluation and structure health monitoring.

**Jishan Zhang** received the master's degree from the Zhengzhou Research Institute of Mechanical Engineering, and the Ph.D. degree in gear fatigue from the Design Unit, Newcastle University, U.K., in 2005. After his graduation from the School of Mechanical Engineering, Hunan University, in 1988, he was a Production Engineer with Dongfanghong Tractor Company, Luoyang, China, for four years. Since 1992, he has been involved in gears while with the Zhengzhou Research Institute of Mechanical Engineering, where he subsequently worked for further five years investigating gear tribology. He has been with the Design Unit, Newcastle University, as a Research Associate. He is currently a Mechanical Engineer and Researcher with over 20 years of experience in geared transmissions. His main research areas include gear material, heat treatment, surface engineering, micropitting, macropitting, scuffing, gear lubrication, and condition monitoring of geared transmissions.

**Brian Shaw** received the Degree in metallurgy from Sheffield University, U.K. He carried out research for his Ph.D. degree with Newcastle University. Since 1993, he has been with the Design Unit, Newcastle University, where he is involved in gear metallurgy, carrying out research on microstructural aspects of the fatigue strength of gear materials. He is the Director of the Design Unit and the Head of Materials Engineering, overseeing materials research, test programs, and consultancy activities. His research includes the investigation of the influence of heat and surface treatments on the bending and contact fatigue strength of carburized, nitride and induction hardened gears, the effect of residual stress, surface texture, and lubricant additives on pitting in gears.

**Aijun Yin** (M'13) received the B.S. degree in mechatronics engineering and the M.S. and Ph.D. degrees from Chongqing University, Chongqing, China, in 2001, 2003, and 2006, respectively. He is currently an Associate Professor with the College of Mechanical Engineering, Chongqing University. His current research interests include machine vision and image processing, intelligent test and instruments, nondestructive testing and evaluation, modern signal analysis and processing, and fault detection and diagnosis.

**Naomi Omoyeni King-Alale** received the B.Sc. degree from the School of Electrical Engineering and Automation, Harbin Engineering University, Harbin, China, in 2013. She is currently pursuing the M.Sc. degree at the University of Electronic Science and Technology of China. Her research includes the investigation on the effect of stress on the magnetic properties and microstructure of electrical steel, and magneto-optical Kerr effect.

AQ:9

AQ:8